Eur. Phys. J. B **60**, 423–433 (2007)
DOI: 10.1140/epjb/e2008-00008-2

THE EUROPEAN PHYSICAL JOURNAL B

Mechanisms of amorphization-induced swelling in silicon carbide: the molecular dynamics answer

M. Bertolus[1,a], F. Ribeiro[1], and M. Defranceschi[2]

[1] Commissariat à l'Énergie Atomique, Direction de l'énergie nucléaire; DEC/SESC/LLCC, Bâtiment 130, CE Cadarache, 13108 Saint-Paul-lez-Durance, France
[2] Commissariat à l'Énergie Atomique, Direction de l'énergie nucléaire; DSOE/RB, Bâtiment 121, CE Saclay, 91191 Gif-sur-Yvette Cedex, France

Received 10 May 2007
Published online 16 January 2008 –

Abstract. We present here the continuation of an investigation of the irradiation-induced swelling of SiC using classical molecular dynamics (CMD) simulations. Heavy ion irradiation has been assumed to affect the material in two successive steps (a) creation of local atomic disorder, modeled by the introduction of extended amorphous areas with various sizes and shapes in a crystalline SiC sample at constant volume (b) induced swelling, determined through relaxation using Molecular Dynamics at constant pressure. This swelling has been computed as a function of the amorphous fraction introduced. Two different definitions of the amorphous fraction were introduced to enable meaningful comparisons of our calculations with experiments and elastic modeling. One definition based on the displacements relative to the ideal lattice positions was used to compare the CMD results with data from experiments combining ion implantations and channeled Rutherford Backscattering analyses. A second definition based on atomic coordination was used to compare the CMD results to those yielded by a simplified elastic model. The results obtained are as follows. On the one hand, comparison of the swelling obtained as a function of the lattice amorphous fraction with the experimental results shows that the melting-quench amorphization simulates the best the irradiation-induced amorphization observed experimentally. This is consistent with the thermal spike phenomenon taking place during ion implantation. On the other hand, disorder analysis at the atomic scale confirms the elastic behavior of the amorphization-induced swelling, in agreement with the comparison with the results of an elastic model. First, no major structural reconstruction occurs during relaxation or annealing. Second, the systems with the most disordered and constrained amorphous area undergo the largest swelling. This means that the disorder and the constraints of the bulk amorphous area are the driving forces for the swelling observed. On the contrary, the nature of the interface does not affect significantly the swelling observed.

PACS. 31.15.Qg Molecular dynamics and other numerical methods – 61.80.Jh Ion radiation effects

1 Introduction

Irradiation-induced swelling has important consequences which can affect considerably the material performance. Several processes at various scales take part to this swelling: creation of point defects, local amorphization, intra or intergranular void creation, gas formation... The influence of the creation of extended disordered or amorphous zones on the material swelling is currently the least well known atomic-scale component of the irradiation-induced swelling. Ion implantation experiments combined with Rutherford Backscattering analysis [1,2] have been performed on silicon carbide. These studies tend to show that material swelling due to amorphization under irradiation is a complex phenomenon. In particular, SiC swelling does not depend linearly on the disorder created in the material, but exhibits two different scalings as a function of this disorder. There are very few studies on amorphization-induced swelling [3,4] and the atomic-scale mechanisms are not well understood. Atomistic modeling can be a powerful tool to shed light on these mechanisms.

We present here the continuation of the investigation of the amorphization-induced swelling using classical molecular dynamics. In this study heavy ion irradiation has been assumed to induce only local amorphization, and to affect the material in two successive steps: (1) creation of local amorphous disorder at constant volume, (2) volume relaxation and induced swelling. The first part of the investigation reported in references [5,6] has yielded several results. First, the good agreement between the molecular dynamics calculations and the experimental results

[a] e-mail: marjorie.bertolus@cea.fr

[5,6] has proven that the modeling chosen for the local amorphization is reasonable, and that the empirical Tersoff potential yields good results for the systems considered. Comparison with an elastic model [6] shows that the amorphization-induced swelling exhibits an elastic behavior. These results have shown that classical molecular dynamics calculations enable one to connect the results of the available experiments with the elastic calculations. They have proved that the two regimes are due to the behavior of the amorphous fraction detected in experiments and have underlined the crucial importance of the definition of the amorphous state at the atomic scale.

The aim of the present paper is to answer the questions left open in the first two papers. In particular we would like to determine whether the structure of the amorphous area and of the interface between the amorphous and crystalline areas has an influence on the results obtained. Then, we would like to confirm the elastic character of the amorphization-induced swelling at the atomic scale. To this aim we have considered various amorphization methods, yielding different amorphous structures and interfaces between amorphous area and crystalline materials. We have then determined the swelling obtained as a function of the disorder introduced for the various conditions. Finally, we have performed a comprehensive analysis of the disorder created and its evolution during relaxation.

The outline of the paper is as follows. We expose first the computational details: the various methods used to partially amorphize the material; the two definitions of the amorphous fraction introduced; and the analyses performed. Then we present the results obtained on the swelling as a function of the amorphous fraction introduced for the various samples constructed, as well as the conclusions of the comparison with the experimental and elastic results. Third, we show the results of the analysis of the structural and chemical disorder in the amorphous area and at the interface between the crystalline and amorphous zones.

2 Computational details and analyses performed

2.1 Atomistic modeling chosen

Heavy ion irradiation has been assumed to affect the material in two successive steps: (a) creation of local atomic disorder, modeled by the introduction of extended amorphous areas with various sizes and shapes in a crystalline SiC sample at constant volume (b) induced swelling, determined through relaxation using Molecular Dynamics at constant pressure. All simulations reported herein were carried out using the classical molecular dynamics simulation code XMD. This code has been developed by Rifkin and is freely available on the web [7]. Results were obtained with the 89' parameterization of Tersoff potential [8]. The validity of this approach has been justified in reference [6].

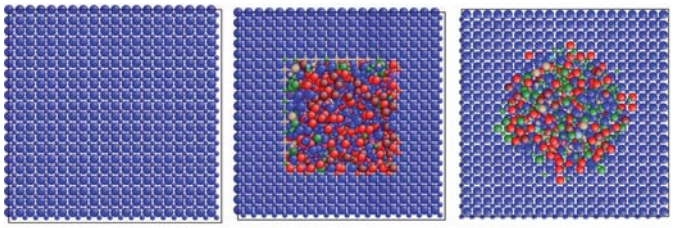

Fig. 1. $10 \times 10 \times 10$ supercell of crystalline β-SiC (a), as well as two composite samples obtained for (b) a cubic cut-pasted amorphous zone and (c) a spherical *in situ* melted-quenched zone. Large and small spheres represent Si and C atoms, respectively. Color coding is done according to coordination number: blue, red, and green correspond to coordination numbers four, five, and three, respectively.

2.2 Local amorphization and relaxation

Three different methods of local amorphization were used to investigate the influence on the swelling observed of the nature of the interface and of the amorphous area. First, a composite sample was constructed by substituting a central area at the center of a crystalline β-SiC supercell with amorphous material. To this aim the central area of the crystal was removed and replaced by a cubic amorphous area containing the same number of atoms and exhibiting approximately the same size and shape as the substituted crystalline area. This amorphous material is cut in a large totally amorphous sample yielded by the melting and quenching of a liquid SiC sample at constant volume, and has the same density as the crystalline phase. This type of local amorphization will be referred to as the cut-paste amorphization.

Second, to determine the influence of the interface structure, we have amorphized the central area of the supercell *in situ*. To do this we have separated the system in two sub-systems. To free ourselves from border and corner effects, central areas with spherical and cubic shape have been considered. The central area is melted at 5500 K during 60 ps and is then quenched to 300 K. It becomes amorphous. The outside area is first fixed at 0 K during the first 60 ps, then quenched to 300 K, and remains crystalline. In this manner the crystalline part of the material is taken into account during the amorphization of the central region. The interface produced is therefore different from the interface yielded by the cut-paste method, and should give a better representation of the system physics. We will refer to this type of composite samples in the following sections as the *in situ* melted-quenched samples. We have represented in Figure 1 a $10 \times 10 \times 10$ supercell of crystalline β-SiC, as well as two composite samples obtained for a cubic cut-pasted amorphous zone and a spherical *in situ* melted-quenched zone.

Third, to study the influence of the nature of the amorphous zone itself and of the internal stresses inside this area, the amorphous area is also created by the random swapping of C and Si atoms inside a localized zone of the

simulation box. These samples will be referred to in the next sections as chemically amorphized samples.

Finally, to study the influence of the internal and interfacial stresses present in the material prior to volume relaxation, the various composite samples have been annealed at 1000 K during 20 ps. The composite samples obtained are finally allowed to relax in the NPT ensemble at 300 K for 400 ps.

2.3 Definition of the amorphous fraction

The first objective of our investigation is to determine the relative volume change $\Delta V/V^0$, or swelling, induced by the introduction of amorphous areas with various sizes in the material. The crucial point is then to determine the proportion of amorphous material. It is not straightforward, however, since there is no unequivocal definition of an amorphous atom, the amorphous state being essentially a collective property. To determine the amorphous fraction as precisely as possible we have therefore chosen to use two different definitions of an amorphous atom.

The first definition of the amorphous fraction, referred to as the lattice amorphous fraction $f_{a\text{lattice}}$, is based on the analysis of the positions of the atoms in the configuration after relaxation compared to their ideal positions in the perfect crystal lattice. We consider as amorphous each atom i for which the atomic displacement relative to the lattice site is greater than a threshold distance α. This displacement is calculated as $dr = |r_i - r_i^0|$, where r_i is the position in the sample after relaxation and r_i^0 the ideal lattice position in a crystal with the same lattice parameter as the relaxed cell. Based on the $r_i - r_i^0$ distribution of atomic positions in β-SiC at 300 K (see Ref. [6]) we have chosen $\alpha = 0.16$ Å. The main objective of this amorphous fraction definition is to enable a direct comparison with the results from Rutherford Back Scattering (RBS) experiments on irradiated SiC-samples. In RBS combined with channeling techniques the monocrystalline substrate is aligned with the incident ion beam. The backscattering yield then depends on the fraction of atoms which are not in lattice sites, and the disordered fraction determined in these experiments is then based on a position criterion. The lattice amorphous fraction is computed after volume relaxation to be consistent with the experiments, which can only access the final state.

The second definition, referred to as the coordination amorphous fraction $f_{a\text{coord}}$ is based on the analysis of the atomic coordination numbers. The coordination numbers are calculated using a distance criterion: C-C, C-Si and Si-Si bonds are considered to be formed if the two atoms involved are closer than 1.70, 2.10, and 2.80 Å, respectively. These thresholds were determined through the analysis of the distance distributions in various Si-C systems. Then only atoms exhibiting exactly four heteronuclear bonds and no homonuclear bond are considered crystalline, all the others being amorphous. We have checked that taking into account bond angles does not modify the value of $f_{a\text{coord}}$. This definition seems the most physical since it is based on interatomic interactions and bonding, which is at the origin of the materials properties. It is not perfect, however, since an atom can exhibit an ideal first coordination sphere, but no order in its second coordination sphere. Such an atom will be wrongly considered as crystalline using this second definition. But tests have shown that the proportion of such atoms is small, $f_{a\text{coord}}$ being equal to 96% in the case of a fully amorphous cell obtained by a melting-quench process. This definition has enabled us to compare the atomistic results with the elastic results since in the latter the amorphous area is characterized by elastic and density properties different from the crystalline ones. It was shown in our previous study that these two amorphous fractions exhibit different behaviors, in particular around the interface between the crystalline and amorphous areas.

We then calculate the amorphous fraction as the ratio of the number of amorphous atoms over the total number of atoms in the simulation box. Both the coordination and lattice amorphous fractions are estimated, compared, and the swelling as a function of both amorphous fractions is determined for all the various amorphization methods used.

2.4 Simulation box and amorphous fractions considered

We have chosen a simulation box with initial dimension $V_0 = 10a \times 10a \times 10a$, where a is the β-SiC lattice parameter at 0 K and equal to 4.32 Å in the potential used. The simulation box contains a constant number of atoms: 8000. Thanks to the periodic boundary conditions used in the program this enables us to model a perfect and infinite SiC monocrystal. The amorphous fractions considered vary from a few percents to 57% for the spherical *in situ* melted-quenched samples, 61% for the chemically amorphized samples, and 76% for the cubic samples. These are the maximal sizes of the amorphous zones enabling us to prevent spurious interactions between images in the periodic boundary conditions.

2.5 Analysis of the structural and chemical disorders

The second objective of this study is to investigate the mechanisms of the amorphization-induced swelling and to identify the driving forces at the atomic scale. To this aim we have analyzed and compared the disorder in the configurations just after the introduction of the amorphous zone and after relaxation. Initial configurations can be seen as the result of the disorder created by the ion bombardment or disintegrations before relaxation has occurred. It is therefore reasonable to assume that these configurations have a physical meaning and contain elements that govern relaxation. Analysis of both initial and relaxed configurations can then bring insight into the driving forces for the observed swelling. We have used various tools to characterize structural properties of the configurations, such as radial and angular distribution functions. We have also

Table 1. Average energy per atom in eV and atomic displacement at 300 K in Å yielded by the classical molecular dynamics calculations for crystalline and totally amorphous SiC obtained through melting/quench before and after volume relaxation.

	Crystalline SiC	Amorphous SiC before relaxation	Amorphous SiC after relaxation
E/at (eV)	–6.18	–4.63	–5.45
dr (Å)	0.05	1.28	1.32

investigated the chemical disorder in analyzing the coordination numbers, the average bond numbers per atoms, and the nature of the bonds formed: heteronuclear or homonuclear. In addition, the AtomEye software [9] was used to visualize the various samples.

2.6 Interface definition

We also want to study the interface region in detail to characterize possible interface effects on the swelling observed. This implies that the interface area can be differentiated from the bulk amorphous and crystalline zones. In order to identify the three different regions of the simulation box we have to use properties which vary between the crystalline and amorphous materials. The amorphous fraction $f_{a\,\mathrm{coord}}$ is an obvious candidate. Furthermore, it can be seen in Table 1 that the average potential energy per atom and the average atomic displacement relative to the lattice site $dr = |r_i - r_i^0|$, where r_i and r_i^0 have the same definition as in paragraph 2.3, are very different in crystalline and totally amorphous SiC.

We have therefore chosen to use these three different quantities and their variation in the simulation cell: the amorphous fraction, the energy per atom and the atomic displacement. These quantities are averaged in successive slices of 1 Å thickness centered in the middle of the simulation box. These slices are delimited by two spheres with radius R and $R+1$ in the case of a spherical amorphous area, and by two cubes with edge length $2R$ and $2(R+1)$ for a cubic amorphous area. Since carbon and silicon atoms alternate in these slices we have separated the energy per atom into the energy per silicon and per carbon atoms. Moreover, both energies per atoms exhibit similarly large variations between the amorphous and crystalline states, we have therefore considered only the energy per silicon atom. The interface is then defined by the transition area between the amorphous and crystalline materials.

3 Results on swelling as a function of the amorphous fraction for the various samples

3.1 Volume change as a function of $f_{a\,\mathrm{lattice}}$ in the various amorphization conditions

Figure 2 shows the swelling yielded by our calculations as a function of $f_{a\,\mathrm{lattice}}$ in the case of the cut-pasted, cubic and spherical *in situ* melted-quenched, chemically amorphized, and annealed samples. The composite samples with a melted-quenched amorphous area (*in situ*, cut-pasted, annealed or not) all exhibit the same qualitative behavior. Two regimes are observed, with a larger slope for large amorphous fractions than for small amorphous fractions. For the chemically amorphized samples two regimes are also observed. The swelling, however, increases faster for small amorphous fractions, and more slowly for large amorphous fractions. It can be seen that the swelling scaling as a function of the lattice amorphous fraction depends only on the nature of the amorphous bulk, melted-quenched or chemically amorphized, but not on the nature of the interface. The comparison with experiments will then be done on two representative configurations: the cubic *in situ* melted-quenched sample, and the chemically amorphized one. This comparison should enable us to determine which composite sample is most representative of the local amorphization created by irradiation.

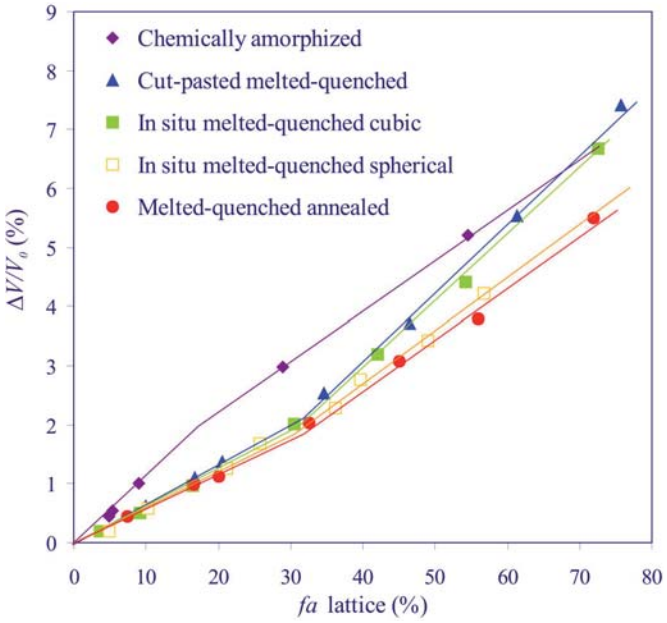

Fig. 2. Swelling as a function of $f_{a\,\mathrm{lattice}}$ in the various amorphization conditions.

The swelling extent itself is more sensitive to the various amorphization parameters than the qualitative behavior, and different swelling values are observed for the various melted-quenched amorphous samples. The swelling obtained depends only slightly on the nature of the interface, but it depends more heavily on the shape of the amorphous area introduced. The cut-pasted composite

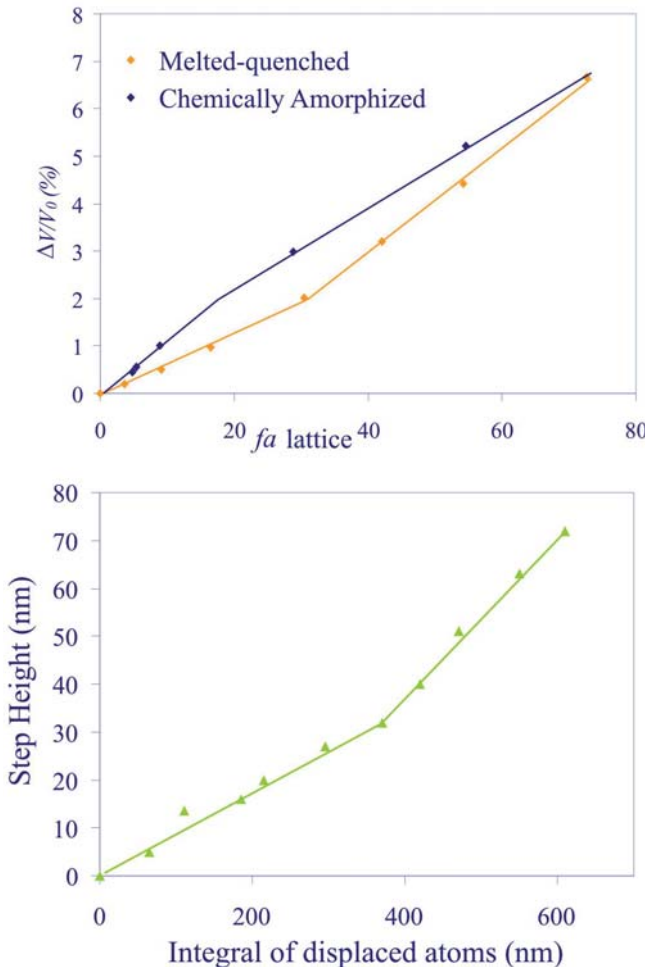

Fig. 3. Comparison of swelling as a function of $f_{a\text{lattice}}$ yielded by (a) Classical molecular dynamics in the case of *in situ* melted-quenched and chemically amorphized samples, and (b) in the ion implantation and RBS experiments by Nipoti [2].

sample leads to a larger swelling than the *in situ* melted-quenched amorphous area. Then, the annealed sample yields the least swelling. In summary, the following order is observed:

$$\Delta V/V^0(\text{chemically amorphized}) > \Delta V/V^0(\text{cut}-\text{pasted}) > \Delta V/V^0(\textit{in situ}\ \text{cubic}) > \Delta V/V^0(\textit{in situ}\ \text{spherical}) > \Delta V/V^0(\text{annealed}). \quad (1)$$

3.2 Comparison with the experiments

Figure 3 shows the relative volume change $\Delta V/V^0$ as a function of the disorder amount determined after relaxation (a) in our molecular dynamics simulations in the case of cubic *in situ* melted-quenched samples and of chemically amorphized ones, (b) in the ion implantation experiments by Nipoti *et al.* [2]. On the experimental curve the disorder amount is expressed as the integral of displaced atoms. This parameter is determined from Rutherford Back Scattering spectra using various channeling approximations, and is assumed to be proportional to the fraction of amorphous material. We have compared these results with the volume variation as a function of $f_{a\text{lattice}}$.

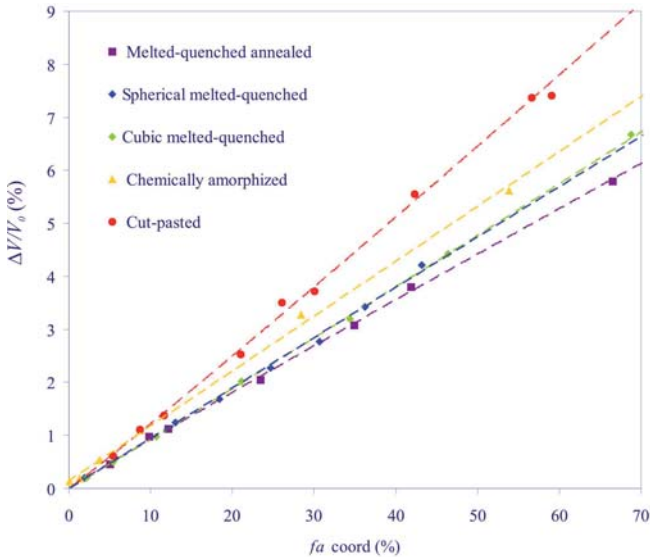

Fig. 4. Swelling as a function of $f_{a\text{coord}}$ in the various amorphization conditions.

Two swelling regimes with different slopes can be observed on all curves. The swelling observed for the chemically amorphized samples, however, does not agree with experimental results, the slope of the first regime being larger than the slope in the second regime. On the contrary, the molecular dynamics results in the case of the melted-quenched composite samples compare very well with the experimental curve. In particular, two different regimes with similar relative slopes are observed in the two curves. The fact that melting-quench amorphization reproduces the best the results of the RBS experiments is consistent with the thermal spike phenomenon [10] that takes place during the slowing down of energetic atoms through elastic collisions. This phenomenon is well known during ion implantation of insulators and has been seen in the atomic scale modeling of displacement cascades. It can be viewed as the short term local melting of the implantation affected region.

3.3 Volume change as a function of $f_{a\text{coord}}$ in the various amorphization conditions

We have then analyzed our results as a function of the coordination amorphous fraction $f_{a\text{coord}}$. Figure 4 shows the relative volume change $\Delta V/V^0$ as a function of the coordination amorphous fraction $f_{a\text{coord}}$ for the cut-pasted, cubic and spherical *in situ* melted-quenched, chemical amorphous and annealed composite samples.

The same qualitative behavior is observed for the various composite samples considered: there is only one regime, and swelling is almost linear as a function of $f_{a\text{coord}}$. The swelling extent, however, depends on the

amorphization condition. It can be seen in Figure 4 that the introduction of a cubic or a spherical amorphous area leads to similar swelling. On the contrary, the chemically amorphized samples lead to a larger swelling than the *in situ* melted-quenched amorphous area, and the cut-pasted samples yield the largest swelling.

In summary the following order is observed:

$$\Delta V/V^0(\text{cut}-\text{pasted}) > \Delta V/V^0(\text{chemically amorphized}) > \Delta V/V^0(\textit{in situ}\ \text{cubic}) > \Delta V/V^0(\textit{in situ}\ \text{spherical}) > \Delta V/V^0(\text{annealed}). \quad (2)$$

The order obtained is slightly different from the one observed in the case of the volume change as a function of $f_{a\text{lattice}}$. In particular, the order is reversed for cut-pasted and chemically amorphized composite samples.

4 Structural and chemical analysis of the composite samples

To get further insight into the swelling mechanisms and confirm the elastic behavior, we have then analyzed the structural and chemical disorder of the interface area and of the amorphous bulk.

4.1 Interface

To investigate the influence of the interface nature, we have compared the *in situ* melted-quenched and cut-pasted composite samples. We have also looked into the effect of volume relaxation and annealing on the interface structure.

4.1.1 Effect of volume relaxation

Almost no difference is observed in the composite samples before and after relaxation. The $g(r)$ distributions before and after relaxation are very similar, differing only by a small shift corresponding to the parameter cell increase. In addition, the coordination numbers vary only slightly during relaxation. Almost no difference is observed in the C coordination, and the variations in Si coordination are small. Only a slight decrease in the amount of Si atoms with high coordination numbers is seen: seven-time coordinated Si atoms disappear, and the number of six-fold coordinated Si decreases to the benefit of tetra-coordinated Si. This is also observed during the volume relaxation of the totally amorphous materials, and indicates that volume relaxation simply enables an elongation of interatomic distances, so that Si atoms considered as bonded before relaxation get further apart and are not considered as bonded any longer after relaxation. We can deduce from these results that there is no major reconstruction of the interface, which is consistent with the elastic behavior. Therefore, only interface properties after volume relaxation are discussed in the following.

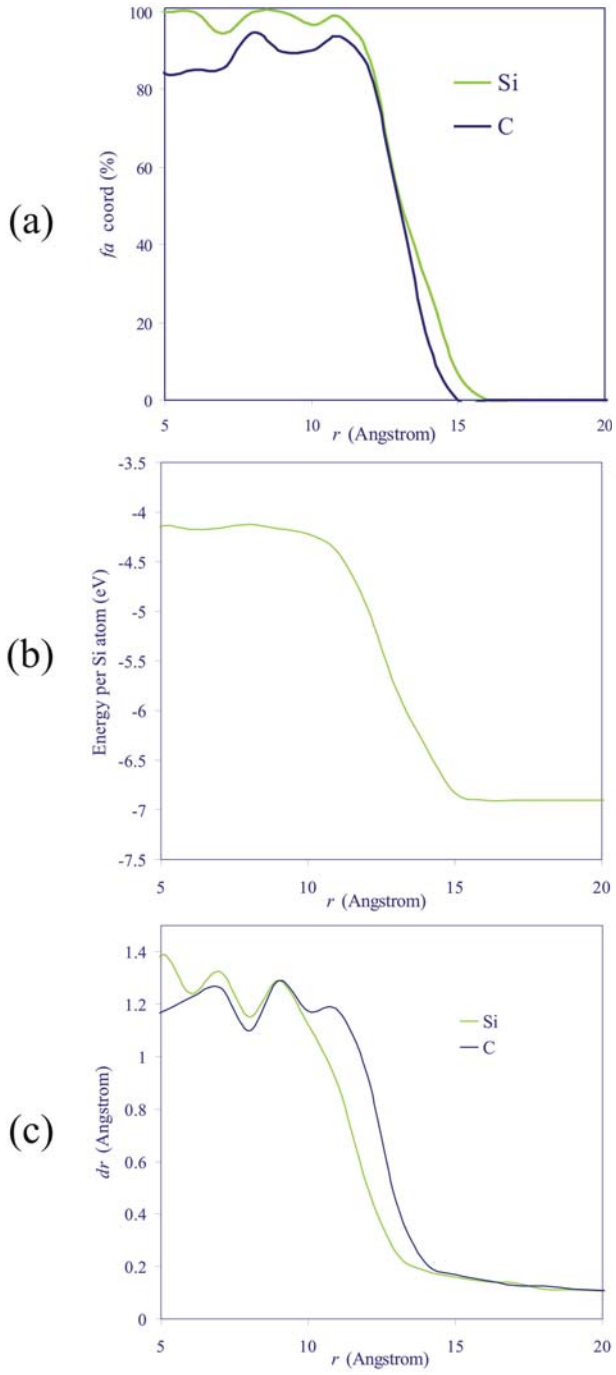

Fig. 5. Definition of the interface using (a) the amorphous fraction, (b) the energy per atom and (c) the atomic displacement in the case of a spherical *in situ* melted-quenched amorphous zone with a $5a$ diameter.

4.1.2 Size of the interface

As shown in the Analyses section, we have chosen a combined analysis of the variation throughout the simulation box of the amorphous fraction, average energy per atom and atomic displacement to determine the thickness of the interface area between crystalline and amorphous material. Figure 5 shows an example of the variation of the

Table 2. Limits and thickness of the crystalline/amorphous interface for the various amorphization methods and representative sizes.

Sample	$f_{a\,\mathrm{coord}}$ (%)	R_{min} (Å)	R_{max} (Å)	Thickness (Å)
In situ	5	6	10	4
melted-quenched	24	14	19	5
cube	35	16	21	5
In situ	5	6	10	4
melted-quenched	20	11	16	5
sphere	33	13	18	5
Annealed	5	6	10	4
melted-quenched	23	15	20	5
sphere	35	17	21	4
	5	8	13	5
Cut-pasted	21	14	20	6
sphere	30	16	21	5

three parameters chosen for a spherical *in situ* melted-quenched amorphous zone with a $5a$ diameter. The crystalline, amorphous and interfacial areas are clearly visible on this figure. The interface is located between the spheres with 11 Å and 16 Å radiuses, and exhibits on average a 5 Å thickness. This confirms that the combination of these three criteria enables us to define unequivocally the interface area.

The thickness obtained for various sizes and composite samples are listed in Table 2. It can be seen that the interface thickness remains approximately constant and equal to 5 Å for all amorphization conditions and all amorphous fractions introduced. In particular, the interface thickness does not increase when the size of the amorphous area increases or during volume relaxation.

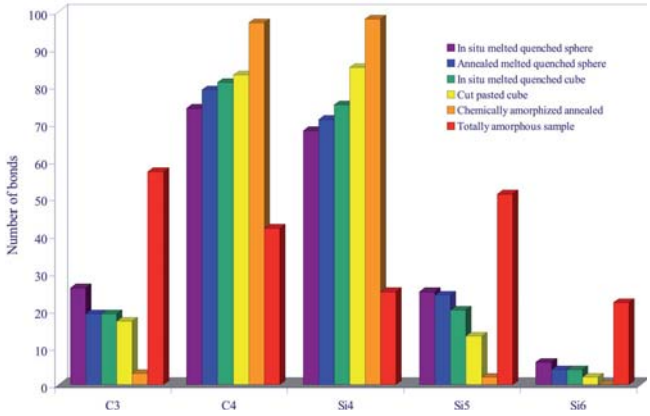

Fig. 6. Interfacial distributions for the various amorphous samples of three and four-time coordinated C, as well as four, five and six-fold coordinated Si.

4.1.3 Bond length distribution in the various interfaces: $g(r)$

A larger first peak is observed in the cut-pasted samples than in the *in situ* melted-quenched samples. Moreover, a larger number of the shortest C-C bonds are observed. Similarly, a slightly larger number of short Si-C bonds are observed for the *in situ* melted-quenched samples. No difference, however, is seen in the Si-Si bonds. The cut-pasted samples therefore exhibit shorter bonds than the *in situ* melted-quenched samples, and are therefore more constrained. The comparison of the C-C bond length distributions for the interfaces and the totally amorphous samples also shows an extra peak corresponding to the Si-C bond length in the $g(r)$ distributions for both interfaces.

4.1.4 Coordination numbers

Average Si and C coordination numbers, as well as the distribution of the various C and Si coordination numbers, have been calculated for the interface area. The average coordination numbers obtained are between 3.7 and 3.8 for C depending on the composite sample and between 4.2 and 4.4 for Si. Only very slight variations are observed between the two interface creation methods, or after annealing. Whatever the method, C is slightly undercoordinated in the interface while Si is overcoordinated. We have represented in Figure 6 the interfacial distributions for the various amorphous samples of three and four-time coordinated C, as well as four, five and six-fold coordinated Si. The analysis of these histograms leads to the following conclusions. First, the C and Si coordination numbers in the interfacial area are similar for all amorphization conditions. Second, the number of over and undercoordinated atoms at the interface is 1/3 to 1/2 the corresponding number in the totally amorphous material, whereas the number of four-time coordinated C and Si is twice or three times larger. The interface structure is therefore closer to the crystal structure.

Third, the number of three-time coordinated C and five-time coordinated Si decreases from the *in situ* spherical amorphous area to the annealed sample to the *in situ*

Table 3. Average number of C-C, Si-C and Si-Si bonds per atom in the interface area, in the perfect crystal and in the totally amorphous material.

Sample	CC	SiC	SiSi
In situ melted-quenched cube	0.3	3.6	0.7
In situ melted-quenched sphere	0.5	3.4	0.9
Cut-pasted cube	0.1	3.8	0.5
Annealed melted-quenched sphere	0.4	3.5	0.7
Chemically amorphized sample	0.5	3.5	0.5
Ref: Perfect Crystal	0	4	0
Ref: Totally amorphous sample	1.3	2.1	3.1

cubic amorphous area to the cut-pasted composite sample. This order is reversed for the four-time coordinated C and Si. This enables the definition of a coordination disorder d_{coord} which varies as follows depending on the amorphization conditions.

$$d_{coord}(\textit{in situ}\ \text{spherical}) > d_{coord}(\text{annealed}) > d_{coord}(\textit{in situ}\ \text{cubic}) > d_{coord}(\text{cut}-\text{pasted}). \quad (3)$$

Comparing this variation to the orders for swelling shown in Sections 3.1 and 3.3 it can be seen that the maximum coordination disorder in the interface does not correspond to maximum swelling.

Fourth, the spherical *in situ* melted-quenched amorphous area leads to more tricoordinated C and pentacoordinated Si and less tetracoordinated atoms than the cubic one. The spherical interface therefore seems to produce more distortion in the lattice and lead to an interface closer to the amorphous sample than the cubic does. This result might be explained by the fact that the cubic amorphous area follows the natural lattice planes, contrary to the spherical one.

Finally, a surprisingly large coordination disorder is observed in the annealed interface. It means that annealing does not enable a recrystallisation of the interface. On the contrary, the cut-pasted interface exhibits very little coordination disorder. Its structure is therefore very close to the crystal structure.

4.1.5 Homonuclear bonds

Table 3 shows the average numbers of C-C, Si-C and Si-Si bonds per atom in the interface area, compared to the perfect crystal and the totally amorphous material calculated using the same parameters.

It can first be observed that the number of homonuclear bonds in the interface remains small: C atoms form on average less than 0.5 homonuclear bond, and Si less than 1 homonuclear bond, compared to 1.3 and 2.1, respectively, in the totally amorphous sample. Therefore, the structure of the interface is also close to the crystal structure as far as the chemical disorder is considered.

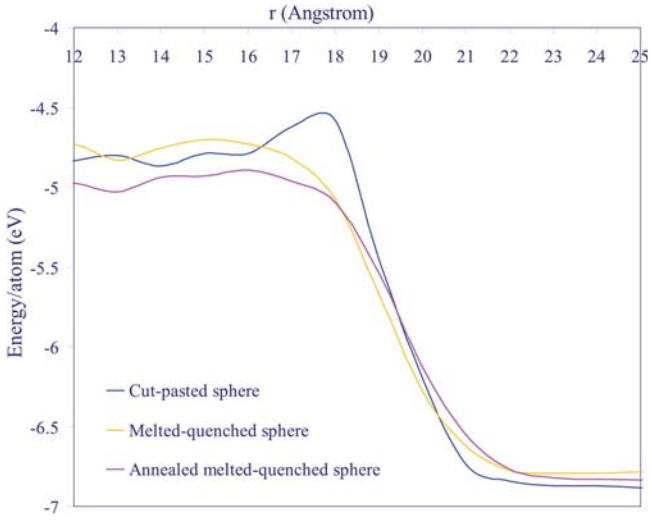

Fig. 7. Average potential energy per silicon atom for *in situ* melted-quenched and cut-pasted areas with a $5a$ diameter.

Second, the order observed as a function of the amorphization condition is as follows:

$$n_{CC}\ (\textit{in situ}\ \text{spherical}) > n_{CC}(\text{annealed}) > n_{CC}(\textit{in situ}\ \text{cubic}) > n_{CC}(\text{cut}-\text{pasted}) \quad (4a)$$

$$n_{SiSi}\ (\textit{in situ}\ \text{spherical}) > n_{SiSi}(\text{annealed}) \approx n_{SiSi}(\textit{in situ}\ \text{cubic}) > n_{SiSi}(\text{cut}-\text{pasted}) \quad (4b)$$

$$n_{SiC}\ (\textit{in situ}\ \text{spherical}) < n_{SiC}(\text{annealed}) < n_{SiC}(\textit{in situ}\ \text{cubic}) < n_{SiC}(\text{cut}-\text{pasted}). \quad (4c)$$

This enables the definition of a chemical disorder d_{chem}, which decreases from the *in situ* spherical amorphous area to the annealed sample to the *in situ* cubic amorphous area to the cut-pasted composite sample. This order is the same as the one observed for the coordination disorder.

4.1.6 Energy per atom

Figure 7 shows the average potential energy per silicon atom in the cases of *in situ* melted-quenched before and after annealing, as well as cut-pasted composite samples. Similar curves are observed for C atoms. A peak with a higher energy (i.e. less negative) is observed in the interface of the cut-pasted samples. The interfaces of the *in situ* melted-quenched samples before or after annealing are more stable and no higher energy peak is observed. This peak proves that the interface created through cutting and pasting is more constraint that the one obtained through *in situ* melting and quenching. Furthermore, the interface before annealing is more constrained than the annealed one.

4.1.7 Conclusion on disorder, constraints and swelling observed

It can be seen that the structural properties of the interface are intermediate between the crystal and the

amorphous ones, but closer to the crystal structure. Moreover, the analysis of the $g(r)$ and of the average energy per atom shows that the cut-pasted interface is more constrained than the interface of the *in situ* melted-quenched sample, as was expected from simple physical arguments. If we combine this result with the swelling observed, we see that the most constrained samples exhibits the largest swelling. This is consistent with an elastic behavior. Finally, the maximum coordination and chemical disorders in the interface of the various samples do not correspond to maximal swelling. The disorder in the interface does not seem to be the driving force for swelling.

4.2 Amorphous bulk

The analysis of the various composite samples shows that the nature of the amorphous bulk is independent from the interface and the crystalline part of the composite sample. Therefore, in order to investigate the influence of the amorphous bulk structure, we have only compared the spherical *in situ* melted-quenched and the chemically amorphized composite samples, as well as looked into the effect of annealing on the amorphous structure.

4.2.1 Effect of volume relaxation

Relaxation yields more modifications in the bulk amorphous area than in the interface. First, in both melted-quenched and chemically amorphized samples, volume relaxation causes a large decrease of the highest coordination numbers of Si atoms (six and seven) in the amorphous bulk to the benefit of tetra and pentacoordinated atoms. C atom coordination numbers, on the contrary, seem unaffected by this relaxation. This result is consistent with an elastic behavior during relaxation: swelling leads to an elongation of interatomic distances without any major reconstruction, as in the interface. Si atoms considered as bonded before relaxation get further apart and are not considered as bonded any longer after relaxation. Relaxation therefore eliminates the constraints due to the high coordination numbers. Second, the $g(r)$ distributions of the melted-quenched samples before and after relaxation are similar. For the chemically amorphized samples, however, there is a significant shift of the C-C and Si-Si peaks from 1.9 Å to 1.65 Å and 2.2 Å, respectively. In the following only the values obtained after relaxation will be discussed.

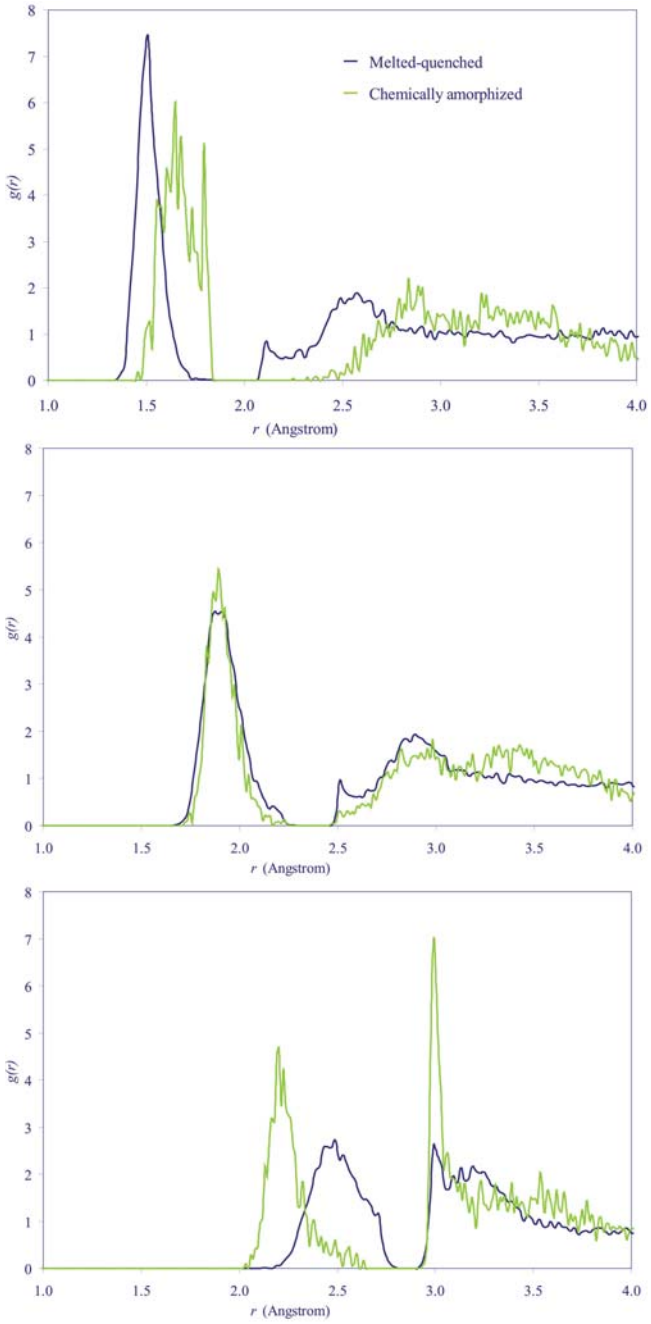

Fig. 8. Radial distribution functions in the amorphous bulk for a spherical *in situ* melted-quenched and a chemically amorphized area with a $5a$ diameter (a) C-C distances, (b) Si-C distances, and (c) Si-Si bonds.

4.2.2 Bond length distribution of the various amorphous bulks: $g(r)$

Figure 8 shows the C-C, Si-C and Si-Si radial distribution functions after relaxation in the amorphous bulk for a spherical *in situ* melted-quenched and a chemically amorphized area with a $5a$ diameter. It can be seen that C-C and Si-Si bond lengths for the chemically amorphized samples are still shifted significantly towards Si-C bond length compared to the melted-quenched samples. This is due to the amorphization method, and means that Si-Si bonds are very short and that C-C bonds are overstretched. The chemical amorphization method therefore seems to create much greater constraints than the melting-quench method, and the system cannot relax into a more physical state, even through annealing. Furthermore, the differences between the two amorphous bulks are considerably

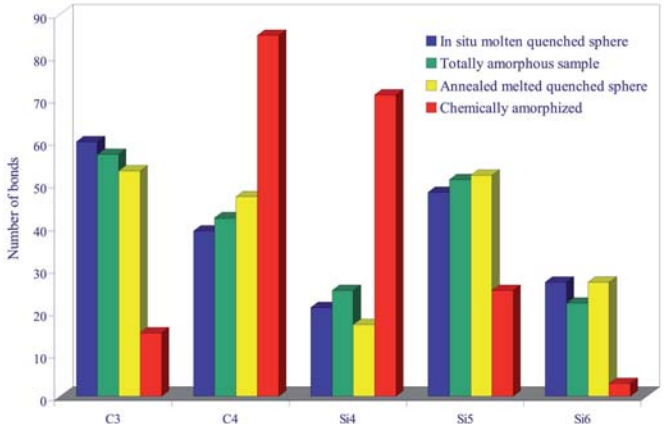

Fig. 9. Amorphous bulk distributions for the various amorphous samples of three and four-time coordinated C, as well as four, five and six-fold coordinated Si.

larger than the differences observed in the various interfaces.

4.2.3 Coordination numbers

Average Si and C coordination numbers, as well as the distributions of the various C and Si coordination numbers, have been calculated for the amorphous bulk. The average coordination numbers obtained for C are between 3.4 and 3.5 for the various *in situ* melted quenched samples before or after annealing, and 3.9 for the chemically amorphized samples. The average coordination numbers for Si are between 5.1 and 5.2 for the various *in situ* melted-quenched samples, and 4.2 for the chemically amorphized samples. The orders as follows are observed in the coordination numbers for C and Si atoms.

$$\overline{cn}_{\mathrm{C}}\ (\mathrm{melted}-\mathrm{quenched}) < \overline{cn}_{\mathrm{C}}(\mathrm{melted}-\mathrm{quenched}\ \mathrm{annealed}) \ll \overline{cn}_{\mathrm{C}}(\mathrm{chemically\ amorphized}) \quad (5a)$$

$$\overline{cn}_{\mathrm{Si}}\ (\mathrm{melted}-\mathrm{quenched}) < \overline{cn}_{\mathrm{Si}}(\mathrm{melted}-\mathrm{quenched}\ \mathrm{annealed}) \ll \overline{cn}_{\mathrm{Si}}(\mathrm{chemically\ amorphized}). \quad (5b)$$

Significant differences are therefore observed between the two amorphization methods, while only slight variations are yielded by annealing. Furthermore, the average coordination numbers for the chemically amorphized samples are very close to four. Similar order relations are observed for the numbers of three and four-time coordinated C and for four, five and six-fold coordinated Si, as represented on Figure 9. This enables the definition of a coordination disorder, as in the case of the interface. This coordination disorder decreases from the melted-quenched samples to the annealed melted-quenched samples to the chemically amorphized samples, which exhibits almost no coordination disorder:

$$d_{coord}(\mathrm{melted}-\mathrm{quenched}) > d_{coord}(\mathrm{melted}-\mathrm{quenched}\ \mathrm{annealed}) > d_{coord}(\mathrm{chemically\ amorphized}). \quad (6)$$

Table 4. Average numbers of C-C, Si-C and Si-Si bonds per atom in the amorphous bulk of the composite sample, and in the totally amorphous material for reference.

Sample	CC	SiC	SiSi
Melted-quenched composite sample	1.3	2.1	3.0
Chemically amorphized sample	2.0	1.8	2.7
Annealed melted-quenched sample	1.2	2.2	3.1
Ref: Totally amorphous sample	1.3	2.1	3.1

4.2.4 Homonuclear bonds

Table 4 shows the average numbers of C-C, Si-C and Si-Si bonds per atom in the amorphous bulk areas for the various composite samples. The similar orders observed in the numbers of C-C and Si-Si bonds and the opposite order observed for the Si-C bonds also enables us to define a chemical disorder, which varies as follows.

$$d_{chem}(\mathrm{melted}-\mathrm{quenched\ annealed}) < d_{chem}(\mathit{in\ situ}\ \mathrm{melted}-\mathrm{quenched}) \ll d_{chem}(\mathrm{chemically}-\mathrm{amorphized}). \quad (7)$$

4.2.5 Conclusion on disorder, constraints, and swelling observed

The analysis of the bond lengths, as well as of the coordination and chemical disorders in the amorphous areas, shows that even if the chemically amorphized samples exhibit almost no coordination disorder due the amorphization method they exhibit more constraints and more chemical disorder than the melted-quenched samples. On the contrary, annealing leads to a slight decrease in structural and chemical disorder. If we combine this with the swelling observed for the various samples, we can see that the systems with the most constrained and disordered amorphous areas swell the most, while the least disordered samples swell the least. This means that the disorder and the constraints of the bulk amorphous area are the driving forces for the swelling observed, contrarily to the nature of the interface. These results confirm the elastic character of the amorphization-induced swelling.

5 Conclusion

Various ways of introducing an amorphous area in crystalline β-SiC through irradiation and the induced swelling have been investigated using classical molecular dynamics.

The swelling has been studied as a function of the amorphous fraction introduced and a thorough analysis of the induced disorder has been carried out.

On the one hand, comparison of the swelling obtained as a function of the lattice amorphous fraction with the experimental results shows that the melting-quench amorphization simulates the best the irradiation-induced amorphization observed experimentally. This is consistent with the thermal spike phenomenon taking place during ion implantation. On the other hand, disorder analysis at the atomic scale confirms the elastic behavior of the amorphization-induced swelling, in agreement with the comparison with the results of an elastic model. First, no major structural reconstruction occurs during relaxation or annealing. Second, the systems with the most disordered and constrained amorphous area undergo the largest swelling. This means that the disorder and the constraints of the bulk amorphous area are the driving forces for the swelling observed. On the contrary, the nature of the interface does not affect significantly the swelling observed.

Finally, our study shows that classical molecular dynamics calculations enabled us to get further insight into the swelling mechanisms in connecting the results of the available experiments with elastic calculations.

References

1. W. Bolse, J. Conrad, T. Rödle, T. Weber, Surf. Coat. Technol. **927**, 74 (1995)
2. R. Nipoti, E. Albertazzi, M. Biancon, R. Lotti, G. Lulli, M. Cervera, A. Carnera, Appl. Phys. Lett. **70**, 3425. (1997)
3. X. Yuan, L.W. Hobbs, Nucl. Instr. Meth. B **191**, 74 (2002)
4. F. Gao, W. Weber, J. Mater. Res. **18**, 1877 (2003)
5. A. Romano, M. Bertolus, M. Defranceschi, S. Yip, Nucl. Instr. Meth. B **202**, 100 (2003)
6. F. Ribeiro, E. Castelier, M. Bertolus, M. Defranceschi, Eur. Phys. J. B **52**, 163 (2006)
7. J. Rifkin, `http://xmd.sourceforge.net (2004)`
8. J. Tersoff, Phys. Rev. B **39**, 5566 (1989)
9. J. Li, Modelling Simul. Mater. Sci. Eng. **11**, 173 (2003)
10. G. Szenes, Phys. Rev. B **51**, 8026 (1995)